A DUAL INVERTER COMBINE BOOST CONVERTER qSBI FOR OPEN-END WINDING INDUCTION MOTOR

To Thanh Loi[1*]

[1]*Binh Thuan community college*

*Corresponding author: thanhloicdcd@gmail.com

(Received September 21, 2020; Accepted January 18, 2021)

Abstract - A Dual boost inverter for open-end winding induction motor has been used to improve the power of the induction motor and reduce the number of power switches. However, this configuration still has many disadvantages: the ac output voltage is less than dc input voltage and switches on the same leg turn on at the same time must be avoided. To solve this problem, this paper presents a dual inverter combine boost converter qSBI for open-end winding induction motor configuration that is used for low energies such as solar energy, fuel cell, and battery. With the proposed configuration, the ac output is higher than the dc input without a DC-DC converter and the switches on the same leg can turn on at the same time. Simulation and experimental results will be presented to demonstrate the new features.

Key words - Open-end winding induction motor; switched boost inverter; Z-source inverter

1. Introduction

In recent years, high-speed electric motor control system requirements have been increasing for electric vehicles [1], new energy sources and motor controlling in the industry. The demand for a high-speed electric motor: lighter-weight, smaller-size and higher-efficiency, has impulsed new designs for electric motors to solve those requirements. However, when operating from small power sources such as solar cells, fuel cells, the basic limiting is the reduction in the current of the source at high speed motor, thus reducing torque and efficiency. Electric vehicles using available battery power are a typical example of a cost and size limitation of the battery. Today, the development of power electronics has solved these limitations with various boost inverter configurations that have been researched and designed to suit each application. And, the algorithms of Maximum Power Point Tracking (MPPT) are used to improve the output power of Photovoltaic systems [10]. A traditional dual inverter configuration (Figure 1) is usually used for open-end winding induction (OWI) motor to improve power, reduce common mode voltage. This scheme needs an open-end winding configuration for the induction motor which is easily obtained by opening the neutral of the stator windings and does not call for any change in the design or structure of the induction motor.

However, this traditional dual inverter still has the limitation that the output voltage is less than the input voltage. We want the output voltage higher than the input to use for low power sources such as solar cells, fuel cells... then we have to add the DC-DC converter in front of the dual inverter. Like traditional inverters, there is still the limitation that both power switches in a leg cannot turn on at the same time because it causes a short circuit DC. source.

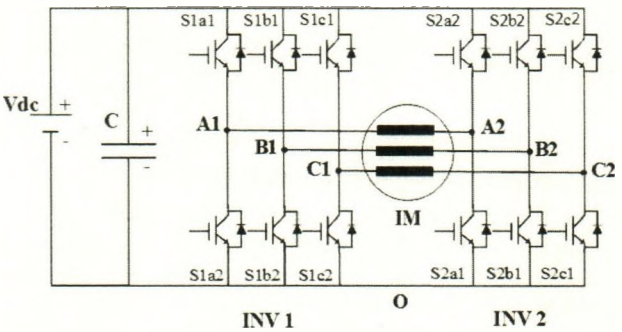

Figure 1. *Schematic of traditional dual inverter*

Thus, the boost inverter has been studied and widely used in practice. In [2], presents the application of the Z source inverter to control electric vehicles using battery or fuel cell by controlling the shoot through duty ratio or modulation index, the fuel cell capacity can be controlled. In [3], describes the dual inverter configuration of the Z source inverter using the pulse width modulation (PWM) method that these two inverters can use either a single dc source or two isolated sources. However, this configuration needs two coils, two capacitors, in increasing the size and cost of the power system, so it is only suitable for applications with high power. For low power applications, many other boost inverter configurations have been proposed. In [4], the switched boost inverter (SBI) configuration uses only one coil, one capacitor, two diodes and one short switch, applied to solar photovoltaic system interfaced micro-grid, the output voltage is adjusted to be greater or smaller than input voltage according to load requirements with a single-stage conversion. In [5], an SBI configuration was modified into quasi-SBI (qSBI) with the advantage of reducing the voltage across the capacitor, increasing the short-circuit ratio and improving the input current. In [6], presents improved SBI configuration reducing the boost voltage factor compared to the traditional SBI, but reducing the cost and the voltage stress on the capacitor. There are also other configurations [7] with different advantages and disadvantages applied to each specific application. Based on the results of the analysis and comparison in [8], the qSBI configuration has many advantages such as current through switches and diode are smaller, the voltage stress on the capacitor, efficiency and the boost voltage factor are higher. Therefore, this paper presents a dual boost inverter for open-end winding induction motor (Figure 2), which increases the output voltage and power switches in a leg can turn on at the same time. Simulation and experiment results verified the analysis.

2. Proposed dual boost inverter

Figure 2 shows the schematic proposed dual boost inverter for open-end winding induction motor, consisting of a network of two diodes, a capacitor, a coil and a power switch connected between the source and the dual inverter.

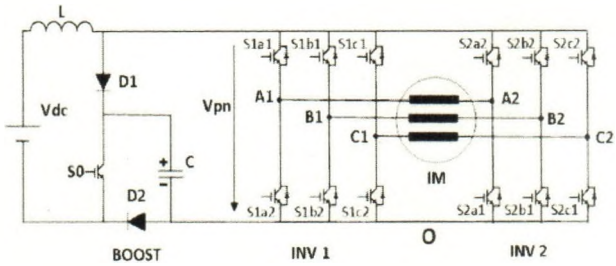

Figure 2. Schematic of proposed dual boost inverter

2.1. Operating principle of the dual inverter

As each phase is two states independently of two switches S1x1 and S2x1 (where x= phase a, b, c), there are four combinations that produce four voltage vectors as shown in Table 1.

Table 1. Four voltage vectors for each phase

Figure3	S1x1	S2x1	Ux
(a)	0	0	$-V_{pn}$
(b)	0	1	0
(c)	1	0	0
(d)	1	1	V_{pn}

Here, "0"= switch is off; "1"= switch is on; x=a,b,c

Figure 3 shows the operating principle of switches for each phase. Two switches S1x1 and S2x1 (S1x2, S2x2 is the opposite rule to S1x2, S2x1, respectively) have four voltage vectors consist of –Vpn, Vpn and two zero voltages.

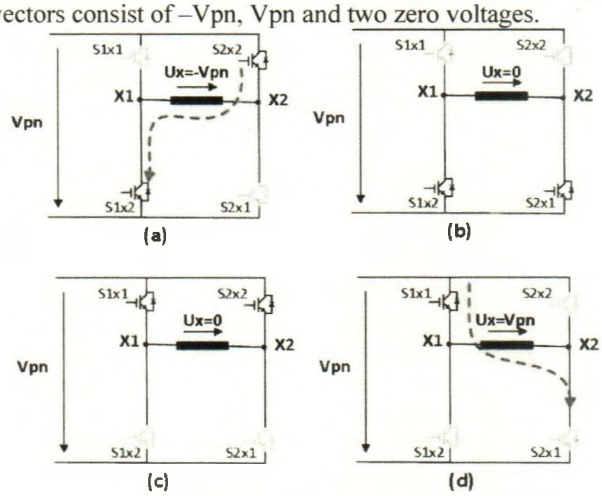

Figure 3. Operating principle of switches for each phase

2.2. The qSBI circuit analysis

For the purpose of analysis, the operating states are simplified into shoot-through and nonshoot-through states as shown in Figure 4 [4].

In the nonshoot-through state shown in Figure 4(a) in the time interval is (1 – D).T, during this state: S0 is turned off, D1 and D2 are turned on, capacitor C is charged from Vdc, whereas inductor L transfers energy from the dc voltage source to the dual inverter, we obtain:

$$\begin{cases} V_L = L\dfrac{di_L}{dt} = V_{dc} - V_C \\ i_C = C\dfrac{dV_C}{dt} = I_L - i_{pn} \end{cases} \quad (1)$$

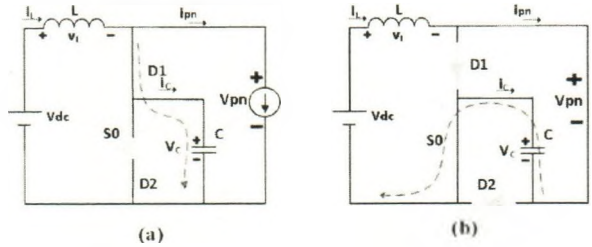

Figure 4. Operating states of qSBI: (a) Nonshoot through, (b) shoot through

In the shoot-through state shown in Figure 4(b) in the time interval is D.T, during this state: S0 is turned on, D1 and D2 are turned off, capacitor C is discharged, whereas inductor L stores energy, we obtain:

$$\begin{cases} V_L = L\dfrac{di_L}{dt} = V_{dc} + V_C \\ i_C = C\dfrac{dV_C}{dt} = -I_L \end{cases} \quad (2)$$

Applying the voltsecond balance principle to L and C in the steady state, (1) and (2) yield

$$\begin{cases} V_C = \dfrac{1}{1-2D} V_{dc} \\ I_{pn} = \dfrac{1-2D}{1-D} I_L \end{cases} \quad (3)$$

The peak dc-link voltage that crosses the dual inverter is expressed in the nonshoot-through state as

$$V_{pn} = V_C \quad (4)$$

The boost factor (B) of the qSBI is calculated:

$$B = \frac{V_{pn}}{V_{dc}} = \frac{1}{1-2D} \quad (5)$$

However, the actual boost factor is higher than the theoretical boost factor because of added dead time of switches.

2.3. PWM control for the proposed dual boost inverter

The frequency of the inductor can be increased to reduce the size of the inductor. This paper shows two PWM control strategies and compares the frequency on the inductor.

Case 1: the PWM control strategy with one shoot-through pulse

Figure 5 shows the PWM control strategy for the proposed configuration with one shoot-through pulse for inverter 1 (INV1). This shoot-through pulse is inserted into the control signal of switches at the same time.

Three phase control waveforms (V1a, V1b, V1c) are compared with a high-frequency triangle waveform (Vtri), to generate control signals for six switches of INV1 (S1a1, S1a2, S1b1, S1b2, S1c1, S1c2). A constant voltage Vsh is compared with a triangle waveform to generate a control signal for the S0 switch. The S0 control signal is inserted into the control signals of six switches (S1a1, S1a2, S1b1, S1b2, S1c1, S1c2) through OR logic gates to generate the

shoot-through states in the dual inverter.

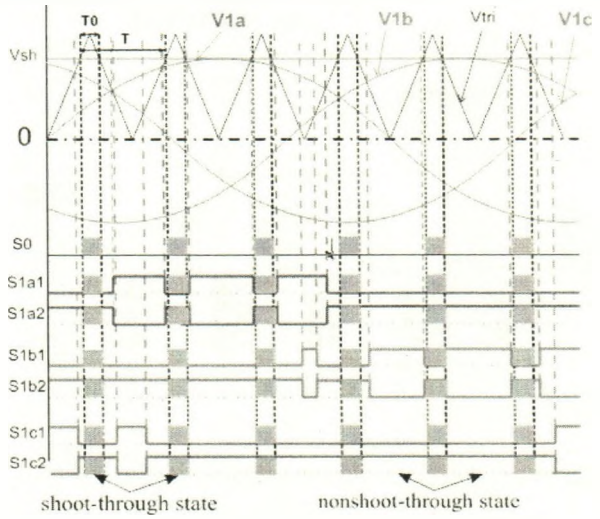

Figure 5. *PWM control strategy for case 1 (INV1)*

Similar to the INV1, three phase control waveforms of the inverter 2 (INV2) (V2a, V2b, V2c shifted 180° to V1a, V1b, V1c, respectively) are compared with Vtri to generate control signals for six switches of INV2 (S2a1, S2a2, S2b1, S2b2, S2c1, S2c2). A constant voltage Vsh is compared with a triangle waveform to generate a control signal for the S0 switch. The S0 control signal is inserted into the control signals of six switches (S2a1, S2a2, S2b1, S2b2, S2c1, S2c2) through OR logic gates to generate the shoot-through states in the dual inverter.

Case 2: the PWM control strategy with two shoot-through pulses

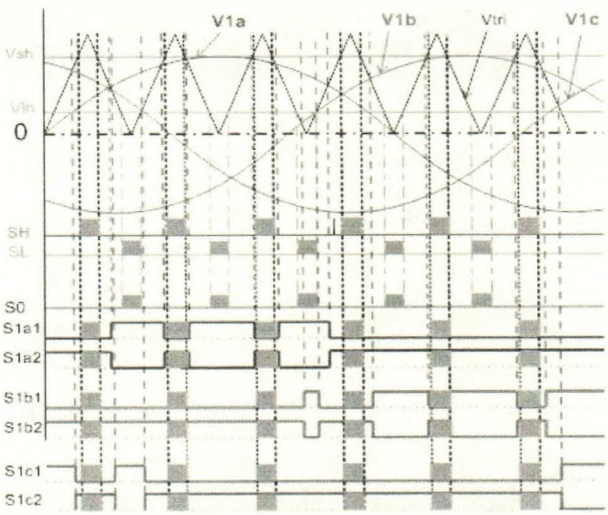

Figure 6. *PWM control strategy for case 2 (INV1)*

Figure 6 shows the PWM control strategy for the proposed configuration with two shoot-through pulses for INV1. A constant voltage Vsh is compared with a triangle waveform to generate an SH control signal, alike Vlh as SL, SH is shifted 180° to SL. The first pulse (SH) is inserted into the control signals of twelve switches of dual inverter. The second pulse (SL) is inserted into the control signal of S0. Operating principle of three phase control waveforms, triangle waveform similar to case 1.

Calculating the values of output ac voltage:

- The peak value of the output ac voltage (Vm) is given by [4]:

$$V_m = M.Vpn = M.B.V_{dc} \quad (6)$$

- The dc–ac inversion voltage gain (G) is defined by [4]

$$G = \frac{V_m}{V_{dc}} = M.B = \frac{M}{2M-1} \quad (7)$$

Where: M is the modulation index.

The relationship between the maximum shoot-through duty ratio (Dm) and the modulation index (M) is Dm=1-M to ensure that the shoot-through interval is only inserted into the traditional zero states.

3. Simulation and experiment results

Table 2. *Experimental parameters of the system*

Input dc voltage	100Vdc
Inductor (L)	1mH
Capacitor (C)	450μF
IGBT S0, the others	G40N120, G30N60
Diode D1, D2	DSEP30-12AR
DSP card	TMS320F28355
The triangle frequency	20 kHz
OEWIM load (simulation with RL load)	0,75 Hp (R=10Ω, L=80mH)

Figure 7 shows a photograph of the experimental system.

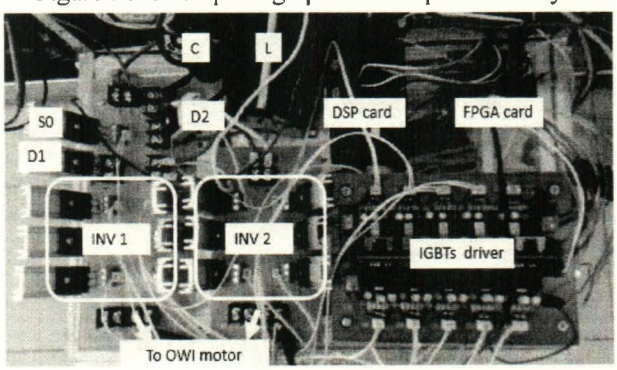

Figure 7. *Experimental system*

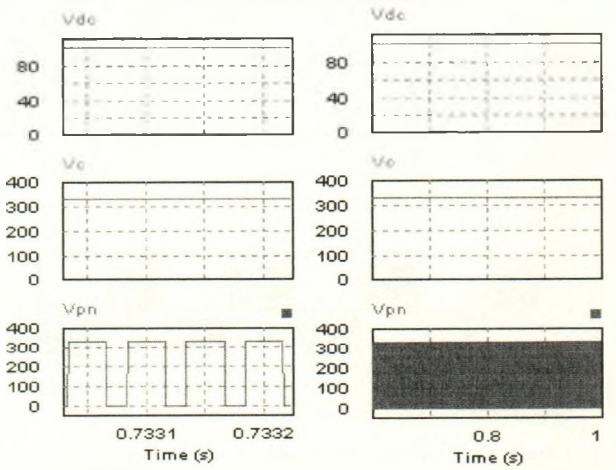

Figure 8. *Simulation results: Input voltage (Vdc); Capacitor voltage (Vc); dc-link voltage (Vpn)*

Figure 8 shows the simulation results for the relationship among input voltage, capacitor voltage and dc-link voltage when M=0.65, D=0.35 and Vdc=100V. We can see that Vc=Vpn= =333V. The theoretical result are caculated by (5) is Vc=B.Vdc=3.33*100V=333V. And Figure 9 shows the experimental results are the same results as theory with Vc=350V. The experimental result is higher than the theoretical result because of added dead time of switches. This is consistent with the theoretical analysis.

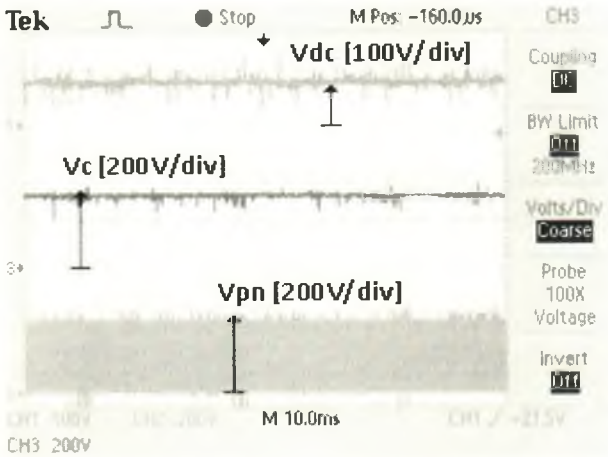

Figure 9. *Experimental results: Input voltage (Vdc); Capacitor voltage (Vc); dc-link voltage (Vpn)*

Figure 10 shows the simulation results for the relationship among input voltage, capacitor voltage and the voltage across the phase windings of the induction machine of phase a. It shows that the amplitude of the voltage across the phase winding equal capacitor voltage or dc-link voltage according to (4) has verified experimental results in Figure 11. The peak dc-link voltage is boosted to 350 V, the peak value of the output voltage is 227.5V and the output ac voltage is 160 Vrms.

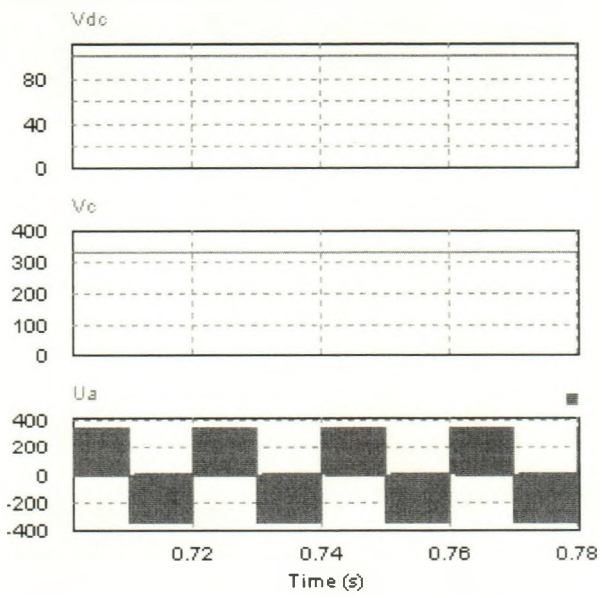

Figure 10. *Experimental results: Input voltage (Vdc); Capacitor voltage (Vc); The voltage across the phase windings of the induction machine of phase a(Ua)*

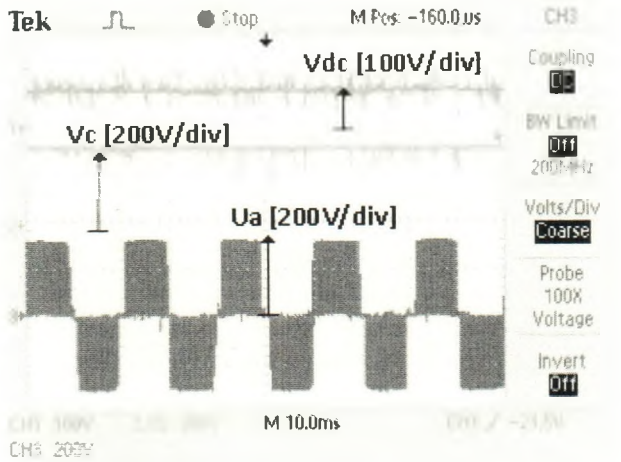

Figure 11. *Experimental results: Input voltage (Vdc); Capacitor voltage (Vc): the voltage across the phase windings of the induction machine of phase a(Ua)*

Figure 12 and Figure 13 show simulation and experimental results for the voltage across there phase windings of the induction machine.

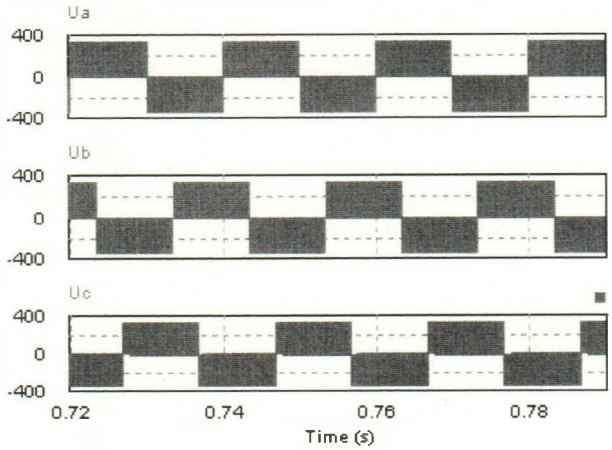

Figure 12. *Simulation results: The voltage across there phase windings of the induction machine*

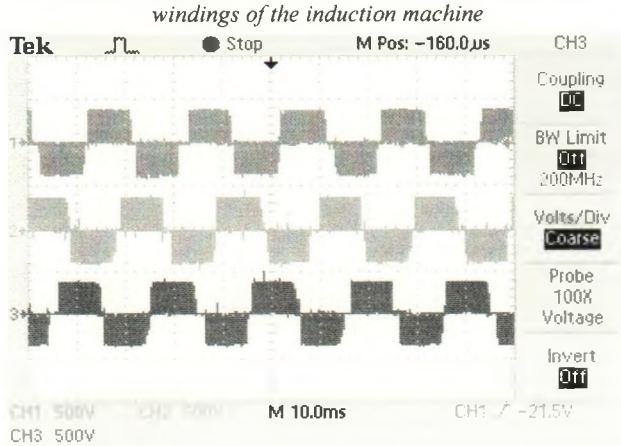

Figure 13. *Experimental results: The voltage across there phase windings of the induction machine*

Figure 14 and Figure 15 show simulation and experimental results that the current flow inductor for PWM control strategy in case 1. We can see that the current flow inductor only store/transfer energy one time in a period.

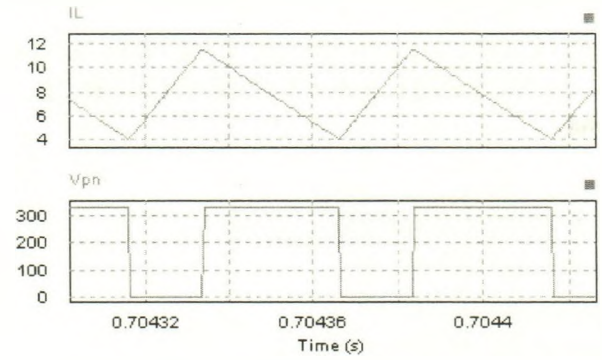

Figure 14. *Simulation results: The current flow inductor (IL) for case 1*

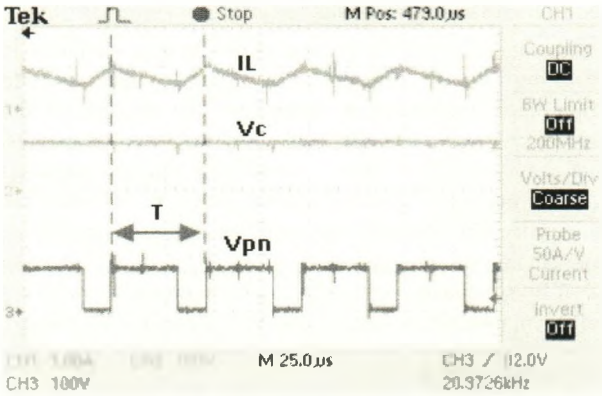

Figure 15. *Experimental results: The current flow inductor (IL) for case 1*

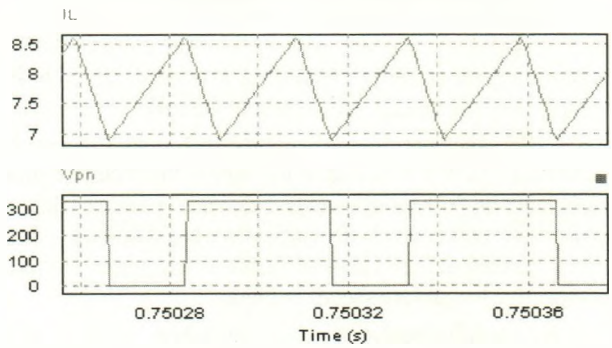

Figure 16. *Simulation results: The current flow inductor (IL) for case 1*

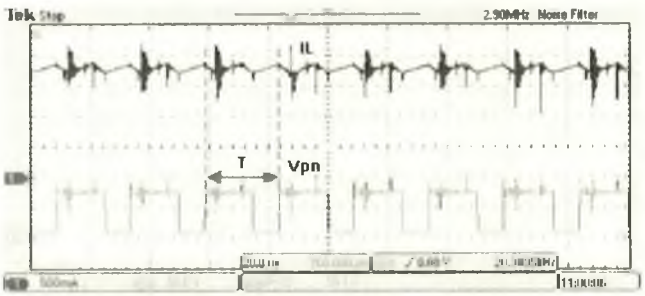

Figure 17. *Experimental results: The current flows inductor (IL) for case 2*

Similarly, Figure 16 and Figure 17 show case 2. We can see that the current flows inductor store/transfer energy two times in a period. So, the frequency of inductor current is double case 1, the ripple of case 2 is reduced to case 1. This is important to reduce the size of the inductor.

4. Conclusion

This paper presents proposed scheme and control algorithm of the proposed dual boost inverter drive system operating an induction machine with open ended windings. Operating principles, analysis and experimental results which have been presented show the following main characteristics:

1) Reducing the number of components in the boost circuit in comparison with the ZSI; it uses one capacitor, two diodes, two inductors and one shoot-through switch.

2) The ac output is higher than the DC input.

3) The switches on the same leg can turn on at the same time, do not care about the deadtime of switches.

4) We can reduce the size of the inductor by increasing frequency shoot-through in a period.

The proposed scheme is applicable to drive open ending winding induction motor from fuel-cell or photovoltaics (PV).

REFERENCES

[1] A. Somani, R. K. Gupta, K. K. Mohapatra and N. Mohan, "Circulating currents in open-end winding PWM ac drives", *IECON 2010 - 36th Annual Conference on IEEE Industrial Electronics Society*, Glendale, AZ, 2010, pp. 798-804.

[2] A. von Jauanne and Haoran Zhang, "A dual-bridge inverter approach to eliminating common-mode voltages and bearing and leakage currents", *in IEEE Transactions on Power Electronics*, vol. 14, no. 1, pp. 43-48, Jan 1999.

[3] M. Alam, J. Jana and H. Saha, "Switched boost inverter applicable for solar photovoltaic system based micro-grid", *2016 2nd International Conference on Control, Instrumentation, Energy & Communication (CIEC)*, Kolkata, 2016, pp. 422-426.

[4] M. K. Nguyen, T. V. Le, S. J. Park, Y. C. Lim, "A Class of Quasi-Switched Boost Inverters". *IEEE transaction on industrial electronics*, vol. 62, no. 3, pp. 1526-1536, March 2015.

[5] N. Minh-Khai, "Cascaded five-level embedded-type switched boost inverter", *J. of Advanced Engineering and Technology.*, vol. 7, no. 9, pp. 107-112, 2014.

[6] F. Gao, P. C. Loh, F. Blaabjerg and D. M. Vilathgamuwa, "Dual Z-source inverter with three-level reduced common-mode switching", *in IEEE Transactions on Industry Applications*, vol. 43, no. 6, pp. 1597-1608, Nov.-dec. 2007.

[7] F. Z. Peng, M. Shen and K. Holland, "Application of Z-Source Inverter for Traction Drive of Fuel Cell—Battery Hybrid Electric Vehicles", *in IEEE Transactions on Power Electronics*, vol. 22, no. 3, pp. 1054-1061, May 2007.

[8] F. Z. Peng, "Z-source inverter", *IEEE Trans. Ind. Appl.*, vol. 39, no. 2, pp. 504-510, March/April 2003.

[9] Y. Jia, S. Zhang, L. Liu, S. Wang and C. Qie, "Improved switching boost inverter", *2016 IEEE 11th Conference on Industrial Electronics and Applications (ICIEA). Hefei, 2016, pp. 2468-2471, 2016.7604007.*

[10] TRAN, Tuan Anh; DUONG, Quan Minh. Design and performance assessment of hybrid-maximum power point tracking algorithm. *Journal of Science and Technology: Issue on Information and Communications Technology*. [S.l.], v. 17, n. 12.2, p. 28-34, dec. 2019. ISSN 1859-1531.